# Mineralogy and pore structure characterization of Lower Oligocene to Early Miocene formations in parts of Assam–Arakan basin, North East India

**Triveni Gogoi[1,2,*], Jenifer Alam[1,3] and Rima Chatterjee[1]**

[1]Indian Institute of Technology (Indian School of Mines), Dhanbad 826 004, India
[2]Wadia Institute of Himalayan Geology, Dehradun 248 001, India
[3]Halliburton, Gurugram 122 018, India

**In this study, reservoir rocks have been characterized by pore-scale measurements and mineralogical analysis of core samples, drill cuttings or crushed samples collected from Upper Assam and Mizoram, North East India. The mineralogical composition and pore types were examined using various laboratory techniques, like petrography under transmitted light microscope, field emission scanning electron microscopy (FE-SEM), X-ray diffraction and nitrogen ($N_2$) gas adsorption. The variation in porosity and permeability was related to different factors such as rock composition, cementing, textural parameters, grain size and sorting, pores and pore throats. Mapping attributes like pore structure, surface area, pore size distribution (PSD), pore orientation, connectivity and pore volume regulated fluid flow through the pore network, which provides significant variations in the reservoir properties. Pores were analysed from the image processing of FE-SEM photomicrographs, which were used to estimate porosity and generate the topology map. This information was further used to visualize pore connectivity in a 3D pore network model. Pore characterization from $N_2$ adsorption analysis helped infer the pore structure, pore volume, and PSD in the reservoir rocks. The studied samples have an excellent meso to macro pore network that is also supplemented by the derived pore network.**

**Keywords:** Mineralogy, pore size distribution, pore network, pore structure, reservoir rocks.

PETROPHYSICS deals with the characterization of reservoirs for their hydrocarbon potential, which is achieved through the evaluation of rock properties both qualitative and quantitatively. The pore structures play a crucial role in controlling the physical properties of porous rocks. Suitability, potentiality, performance and economics of the reservoirs depend on pore connectivity, pore openings, pore structure and gas diffusion characteristics. Pores can be classified based on their diameter as micropore (<2 nm), mesopores (2–50 nm) and macropores (>50 nm), according to the International Union of Pure and Applied Chemistry (IUPAC) classification[1]. The type of pores and pore structure is important in micro- to macro-scale evaluation of reservoirs. This study deals with the pore-scale characterization of reservoir rocks by estimating the surface area, pore size distribution (PSD), pore volume, pore structure, pore connectivity, orientation and mineralogical composition. These properties significantly impact hydrocarbon storage capacity and transport mechanism in reservoir rocks[2]. The rock samples have been examined using an optical microscope, field emission scanning electron microscopy (FE-SEM), low-pressure nitrogen ($N_2$) adsorption technique and X-ray diffraction (XRD).

*For correspondence. (e-mail: triveni.dbr@gmail.com)

## Study area: geological settings

The study area is distributed in parts of Mizoram and Upper Assam of North East India, belonging to the Assam and Assam–Arakan basins. Figure 1 shows these two study areas along with the well locations used for this study. The Upper Assam Basin and the Assam–Arakan thrust belt hold a similar Tertiary stratigraphy with slight variations[3]. The Assam Basin is bounded in the northwest by the Eastern Himalayan fold belt, in the southeast by the Naga–Schuppen belt and in the southwest by the Mikir Hills[4,5]. The Barail group of the Oligocene age is the main producing reservoir in Upper Assam Basin, which is further divided as the Lower Barail Arenaceous Formation and the coal-shale unit of Upper Barail Argillaceous Formation[6]. The Neogene sediments of Surma Group cover the entire state of Mizoram. Sediments of marine siliciclastic deposits dominated by sandstone and a silty shale succession from the Late Oligocene to Late Miocene age belong to the Surma Group[7]. This Group has been subdivided into the Bhuban Subgroup (Lower, Middle and Upper Bhuban Formations) and Bokabil Formation mainly based on the relative abundance of shale and sandstone[8,9].

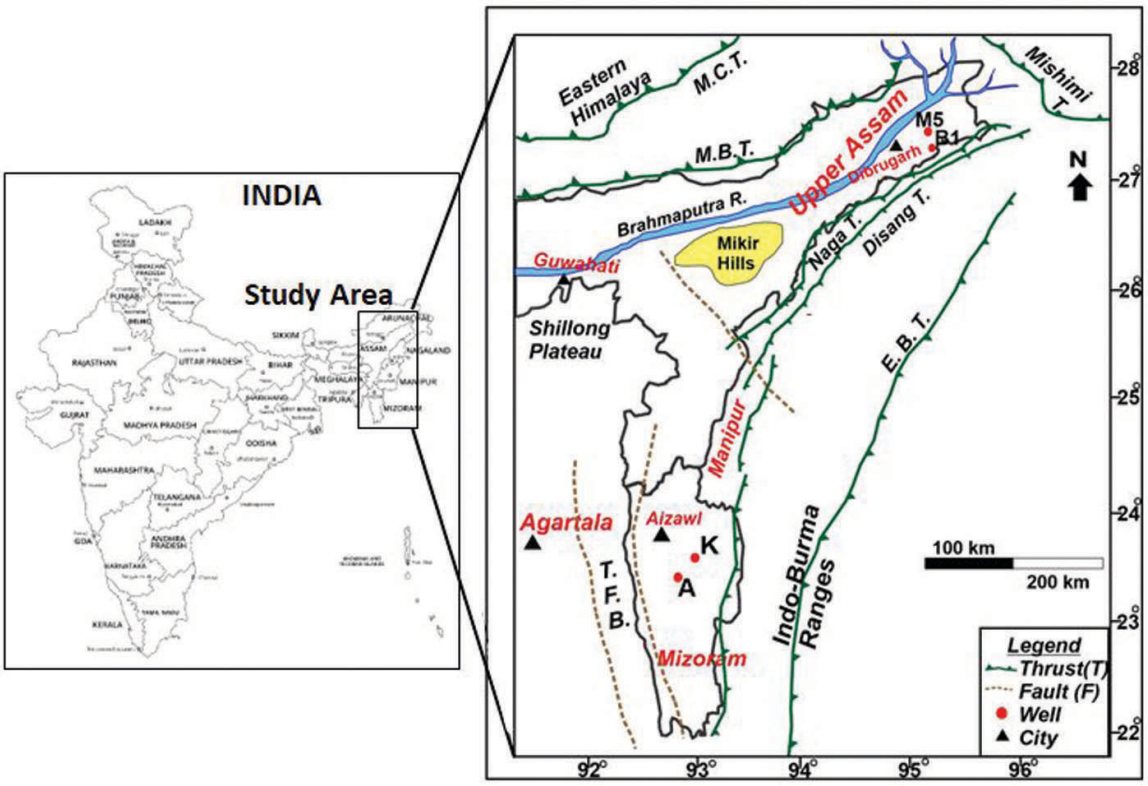


**Figure 1.** Map showing the study area (black rectangle) in Upper Assam and Mizoram, North East India. The well locations (M5, B1, A and K) are marked by red circles. (MBT, Main Boundary Thrust; MCT, Main Central Thrust; TFB, Tripura Fold Belt; EBT, Eastern Boundary Thrust).

## Materials and methods

Ten core samples were collected within a depth interval of 4059–4069 m from well B1 situated in a sub-thrust zone and 2681.8–2690.0 m from well M5 situated in a normal faulted region. These two depth intervals lie in the Lower Barail Formation of Oligocene in Upper Assam. Log responses of wells M5 and B1 show that the target depth intervals mainly comprise sandstone with a few bands of shale (Figure 2 *a* and *b*) respectively. Drill-cuttings of shaly sand samples were collected from two wells (A and K) of Mizoram belonging to the Bhuban Formation of Early to Middle Miocene. These samples were crushed and prepared according to the standard specifications of individual analysis techniques as described below.

### *Petrographic study*

Thin sections were prepared for eight samples of Upper Assam and examined under a microscope (Leica MPV II). Identification of different minerals, rock texture, secondary infillings in pores and cementing material was carried out. Photomicrographs representing the distinct identified features were taken using the attached camera at 5 megapixels.

### *Field emission scanning electron microscopy analysis*

FE-SEM is being used by several researchers to study minerals, texture, pore geometry, pore size, clay type and the influence of diagenetic effects on reservoir rocks[10]. A focused beam of high-energy electrons interacts with the samples producing signals that provide information about the external morphology, mineral grains and structure of the materials. FE-SEM studies were carried out on ten core samples (five each from wells B1 and M5) of Upper Assam and 14 drill cutting samples (five from well A and nine from well K) of Mizoram. About 1 mm chips of each sample were separated and dried overnight in a low-temperature (<60°C) drying oven to avoid moisture effects during FE-SEM analysis. The dried sample chips were then coated with a conductive metal like gold. A scanning electron microscope (Supra 55 Carl Zeiss) was used for analyses. The samples were scanned and the corresponding photomicrographs were collected under magnification ranging from 5000× to 50,000×.

### *Powder X-ray diffraction analysis*

In an X-ray diffractometer, the sample rotates at an angle $\theta$ in the path of a collimated X-ray beam. The intensity

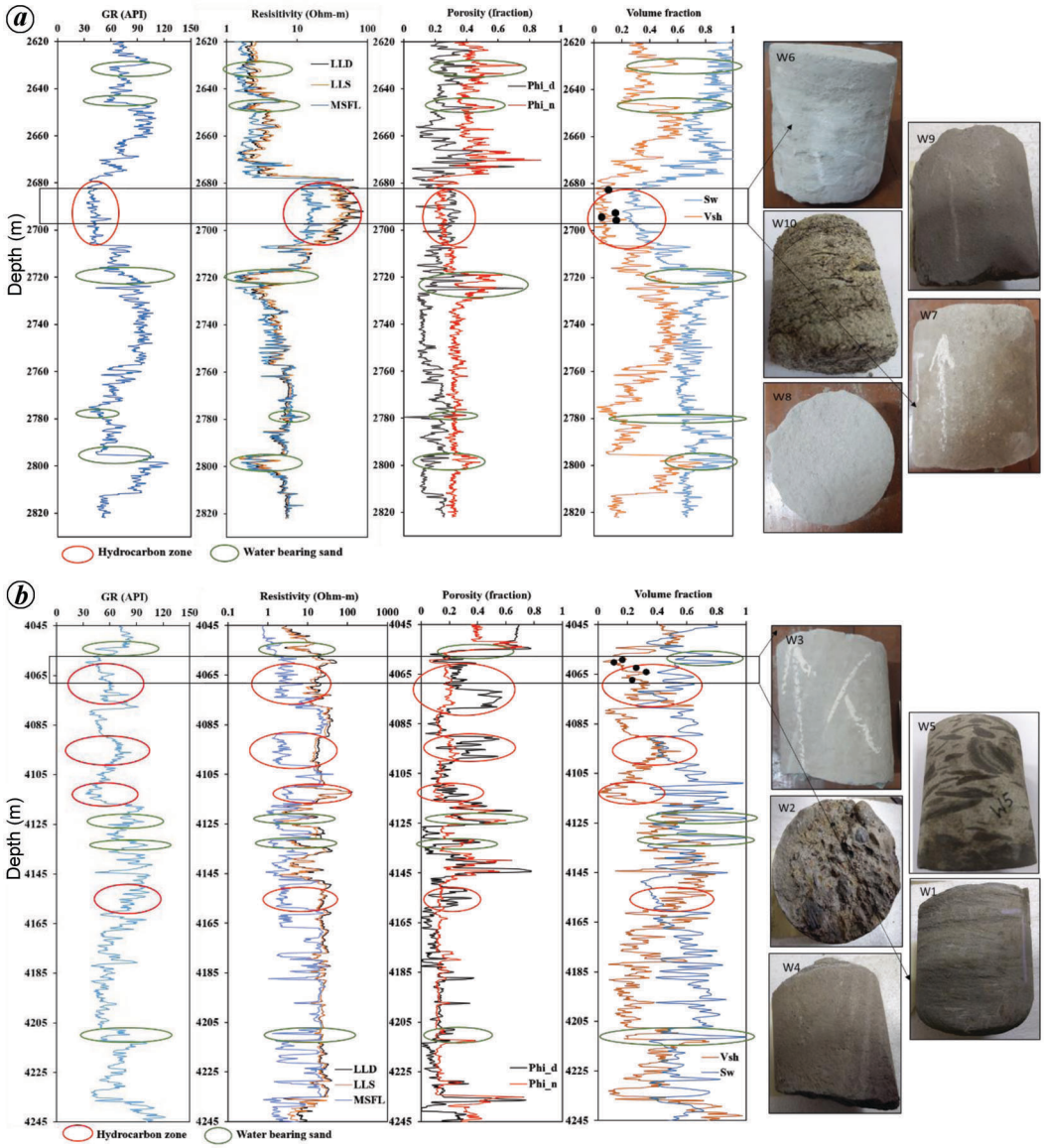


**Figure 2.** Well log response for specific depth intervals of wells (***a***) M5 and (***b***) B1 along with the photographs of core samples. The core plugs are perpendicular to the bedding/laminations. Black dots show fraction of clay minerals from rock samples. The red and green ellipses indicate signatures of hydrocarbon and water-bearing sands. GR, Gamma ray; LLD, Laterolog deep; LLS, Laterolog shallow; MSFL, Microspherically focused log; Phi_d, Density porosity; Phi_n, Neutron porosity; $V_{sh}$, Volume of shale; $S_w$, Water saturation.

of the reflected X-rays records a peak when there is a constructive interference of incident X-rays. These signals are converted to a count rate. An international organization, the Joint Committee on Powder Diffraction Standards (JCPDS), has compiled the pattern of intensity peaks of minerals at a specified angle ($2\theta$). Mineral identification is carried out by plotting the X-ray diffraction (XRD) counts against $2\theta$ angle, and comparing the peaks with the standard set of JCPDS. XRD analyses were carried out on ten core samples (five each from wells M5 and B1) of Upper Assam and 56 rock-cutting samples (47 from well A and 9 from well K) of Mizoram. The crushed samples were passed through a 72-mesh size (212 μm) sieve and dried in the oven for about 1–2 h at <60°C before XRD analysis. An X-ray diffractometer (Panalytical X'PERT PRO) equipped with a ceramic copper X-ray tube was used for XRD analyses of the samples.

### *Low pressure nitrogen adsorption analysis*

The low-pressure nitrogen ($N_2$) adsorption and desorption isotherms were determined (micromeritics system; model: 3FLEX 3500). Ten samples from Upper Assam and 12 from Mizoram were selected for analysis. Part of the core samples was crushed manually and sieved through a 1.0–1.2 mm

**Table 1.** Petrographic study in the Barail Formation of Upper Assam, India

| Sample | Depth (m) | Petrography |
|---|---|---|
| Well B1 | | |
| W1 | 4068.1–4068.2 | Laminated features; very fine grained; poorly sorted; tightly packed; subrounded; line contact; quartz, feldspar, clay, pyrite, rock fragments, clay cement. |
| W2 | 4060.4–4060.5 | Medium to fine grained; poorly sorted; moderately packed; subrounded; point and line contact; quartz, feldspar, muscovite, rock fragments, clay, ferruginous cement. |
| W3 | 4059.8–4059.9 | Very fine grained; poorly sorted; tightly packed; subrounded; line contact; quartz, feldspar, rock fragments, clay, ferruginous cement. |
| W5 | 4064.6–4064.7 | Coarse to medium and fine to very fine grained bands presents; moderately packed; angular and subrounded; line contact, concavo convex and point contact; quartz, feldspar, rock fragments, muscovite, pyrite, magnetite, clay, siliceous cement. |
| Well M5 | | |
| W6 | 2681.8–2682.0 | Medium to fine grained; poorly sorted; moderately packed; subrounded; point, line, concavo convex and sutured contact; quartz, feldspar, rock fragments, muscovite, pyrite, clay. |
| W7 | 2689.7–2689.8 | Fine-grained; moderate to well sorted; moderate to loose packing; angular; line and point contact; quartz, muscovite, feldspar (plagioclase), rock fragment, clay, siliceous cement. |
| W8 | 2686.3–2686.4 | Fine to medium grained; poor to moderately sorted; poorly packed; subangular; point contact; quartz, feldspar, clay, heavy minerals, pyrite; ferruginous cement. |
| W9 | 2686.8–2686.9 | Fine to medium grained; moderately packing; subrounded; line and point contact; quartz, feldspar, rock fragments, pyrite, muscovite, clay, ferruginous cement. |

sieve screen. About 1–2 g of these samples was dried to remove the surface moisture at 105° ± 5°C for 2–4 h in a vacuum oven. Subsequently, the sample was placed in a sample cell and degassed under a vacuum at 200°C. The pressure maintained during adsorption was less than 760 mmHg. The amount of nitrogen adsorbed was recorded with pressure indicated by the isotherm curve[11]. The surface area was calculated from the adsorption curve following Brunauer–Emmet–Teller (BET) theory[12]. The adsorption data were interpreted using Barrett, Joyner and Halenda (BJH) inversion method to estimate PSD and pore volume[13,14].

## Results and discussion

On the basis of the above-mentioned laboratory experiments, the characteristics of the reservoir rocks were evaluated. Pore structure and mineralogy play a major role in hydrocarbon storage capacity and transport mechanism in reservoir rocks[15].

### *Petrographical and mineralogical characterization*

The petrographical study was carried out to estimate grain size, sorting, contact type, roundness, matrix and pore-filling minerals (Table 1). The grain distribution in samples of well B1 was very fine to medium grains and poorly sorted, whereas moderately sorted fine to medium grains were found in well M5. The main mineral constituents were quartz, feldspar, muscovite, clay minerals, rock fragments and framboidal pyrite. Photomicrographs of some samples showed quartz-rich reservoir rocks and pores partially filled with clay minerals (fine brown coloured; Figure 3). Most grains were irregular and rectangular, indicating that the sediments had travelled a short distance under low energy conditions.

Figure 4 shows FE-SEM photomicrographs of some samples from Barail Arenaceous Formation of Upper Assam. Kaolinite having book-like plates, is the dominant clay mineral in almost all the samples. Quartz crystal overgrowths are observed in W2 and W7, which are inhibited by clay formation. Pyrite is distinctly visible in W9, which is coated with smectite. Muscovite is present in massive amounts in the studied area. Figure 5 shows FE-SEM images of samples A1, A3 from well A and K2, K4 and K8 from well K belonging to the Bhuban Formation of Mizoram. These photomicrographs mostly display clay morphology featuring ragged and fleecy edges, with a large proportion of kaolinite, illite and chlorite. Petrophysical evaluations with high clay may underestimate the saturation of hydrocarbons. Intergranular pores are dominantly present in these samples. The presence of pyrite crystals is detected in K2. Pyrite is distinctly visible in samples W9 and K2. FE-SEM photomicrographs show the presence of quartz overgrowths in most of the samples of Upper Assam (e.g. W2, W7). The predominant clay type is kaolinite which is present in almost all the samples. Illite is also a dominating clay mineral in Mizoram. Petrophysical evaluations with high clay may underestimate the saturation of hydrocarbons. Figure 6 shows a typical example of interpreting distinct peaks of minerals in X-ray diffractograms at a depth interval of 1260–1262 m (K4) of well K. Table 2 lists the computed mineral contents from the ten samples

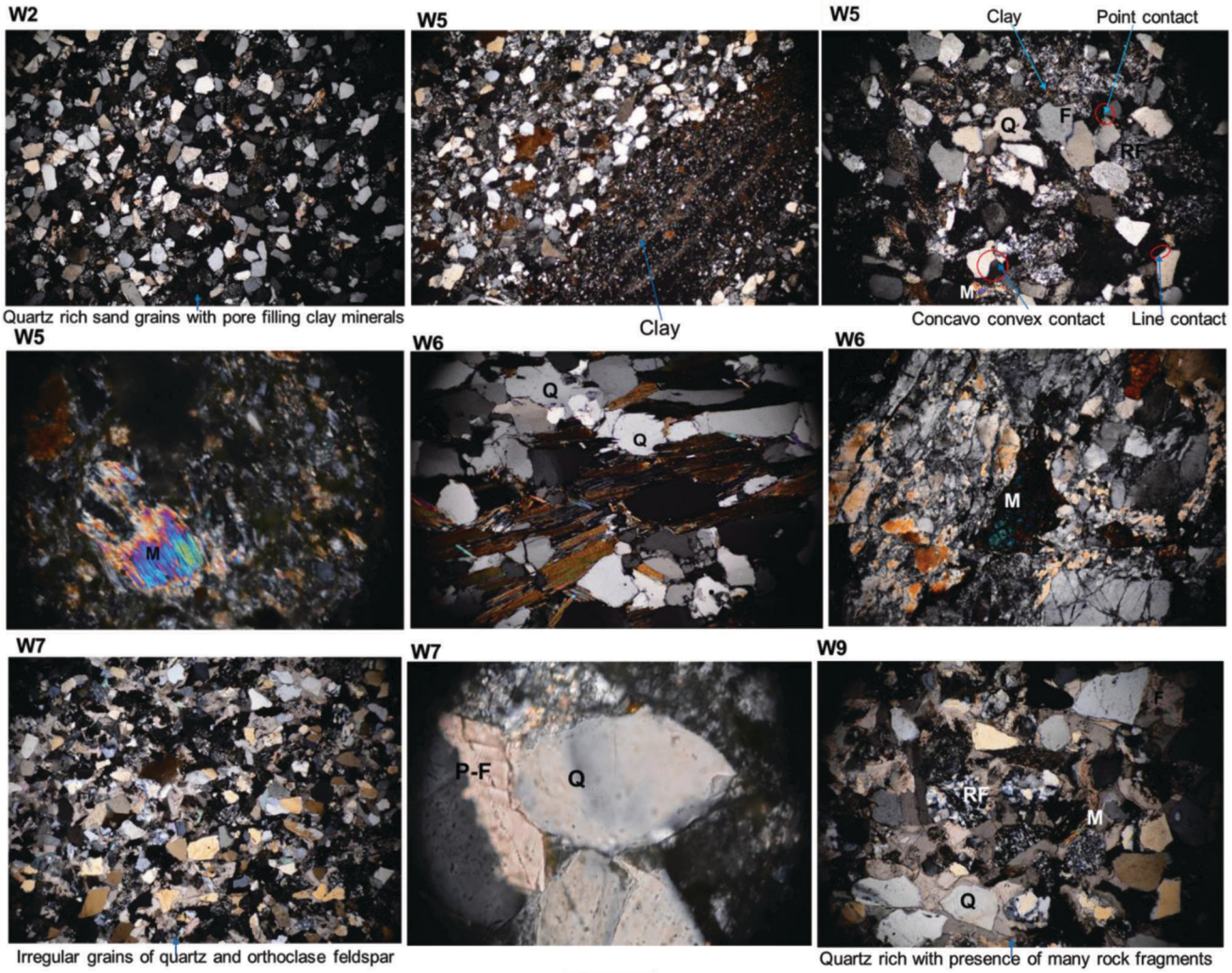


**Figure 3.** Thin-section photomicrographs of samples from Upper Assam (Q, Quartz; F, Feldspar; M, Muscovite; P–F, Plagioclase feldspar; RF, Rock fragments).

of Upper Assam[9]. The average quartz content is 43.12% in Upper Assam. Similarly, mineral quantification from the cutting samples of Mizoram[9] indicates clay mineral in the range 2.24%–52.49%, quartz 29.35%–78.33%, and feldspar 4.22%–11.55% (ref. 9). Significant amounts of muscovite and heavy minerals are detected with an average of 8.47% and 5.18% in Upper Assam and 6.68% and 8.53% in Mizoram respectively[9]. The carbonate content is low compared to other minerals. The clay minerals determined by XRD are kaolinite, illite and chlorite. In Figure 2, the total fraction of clay from XRD has been plotted on the log predicted volume of the shale curve as black dots. Both values are well correlated.

### *Pore structure characterization from FE-SEM image processing*

The FE-SEM photomicrographs were processed to evaluate pore structure, size, orientation, connectivity, deepness, and area to determine the flow mechanism. Dark pixels represented lower attenuation, i.e. porous regions, while lighter pixels denoted highs or peaks in the grey-scale photographs[16]. Images were processed using an image processing software (Optimas version 6.51). The pores were identified and outlined by setting a threshold value of greyscale in the photographs of W2, W6 from Upper Assam and A2, K4 from Mizoram (Figure 7 *a*). Figure 7 *b* and *c* shows the centre of the pores and pore structure and its orientation respectively. It can be seen that most of the pores are oriented in a uniform pattern. The pore network model of Fatt *et al.*[17] has been used extensively in recent decades as it can account for detailed pore-scale heterogeneity. The 3D visualization of FE-SEM images was based on the topographic-intensity map from image processing[18]. The length and height (or depth) of the pores were measured and displayed in 3D form. This illustrates the pore surface morphology, where the pore deepness gradually changes from red to blue on the colour scale (Figure 7 *d*).

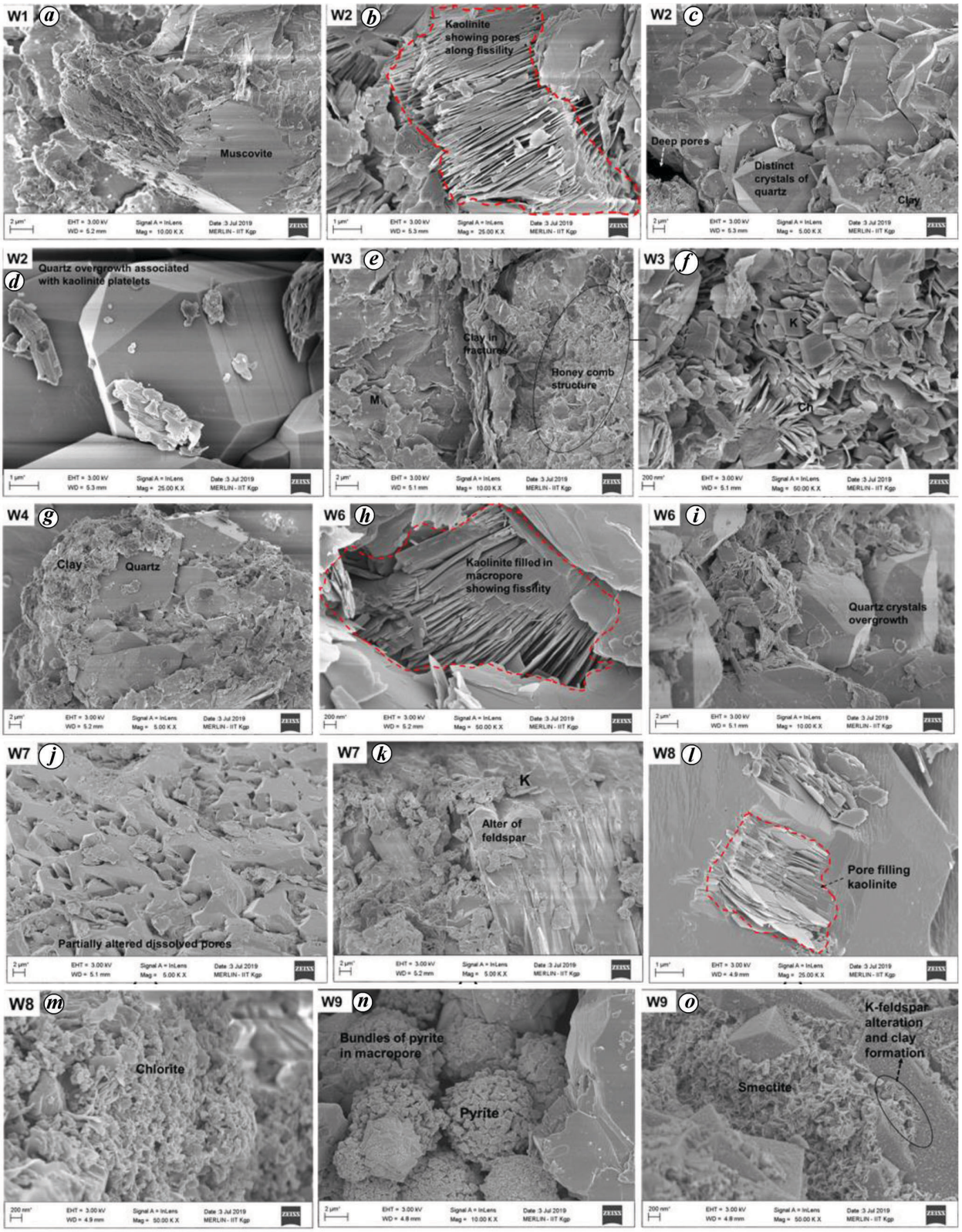


**Figure 4.** FE-SEM photomicrographs from Upper Assam showing (***a***) muscovite (M) and clay; (***b***) interlayer pores in fissile plains of kaolinite; (***c***) cluster of quartz crystal overgrowths (5–10 µm) associated with clay formation; (***d***) quartz overgrowth associated with kaolinite platelet; (***e***) honeycomb structure (black ellipse) associated with platy chlorite (ch), irregular, individual books of blocky kaolinite (K); (***f***) flake-like illite platelets and kaolinite oriented parallel to each other in fractures; (***g***) quartz crystals covered with clay; (***h***) fissility book structure of kaolinite filled in macropore; (***i***) well-developed quartz crystal overgrowths; (***j***) partially altered dissolved pores; (***k***) flakes and books of kaolinite (K) partially covering the altered feldspar grains; (***l***) pore filling kaolinite; (***m***) chlorite; (***n***) framboidal pyrite with smectite coating; (***o***) leached grains of K-feldspar associated with the formation of smectite.

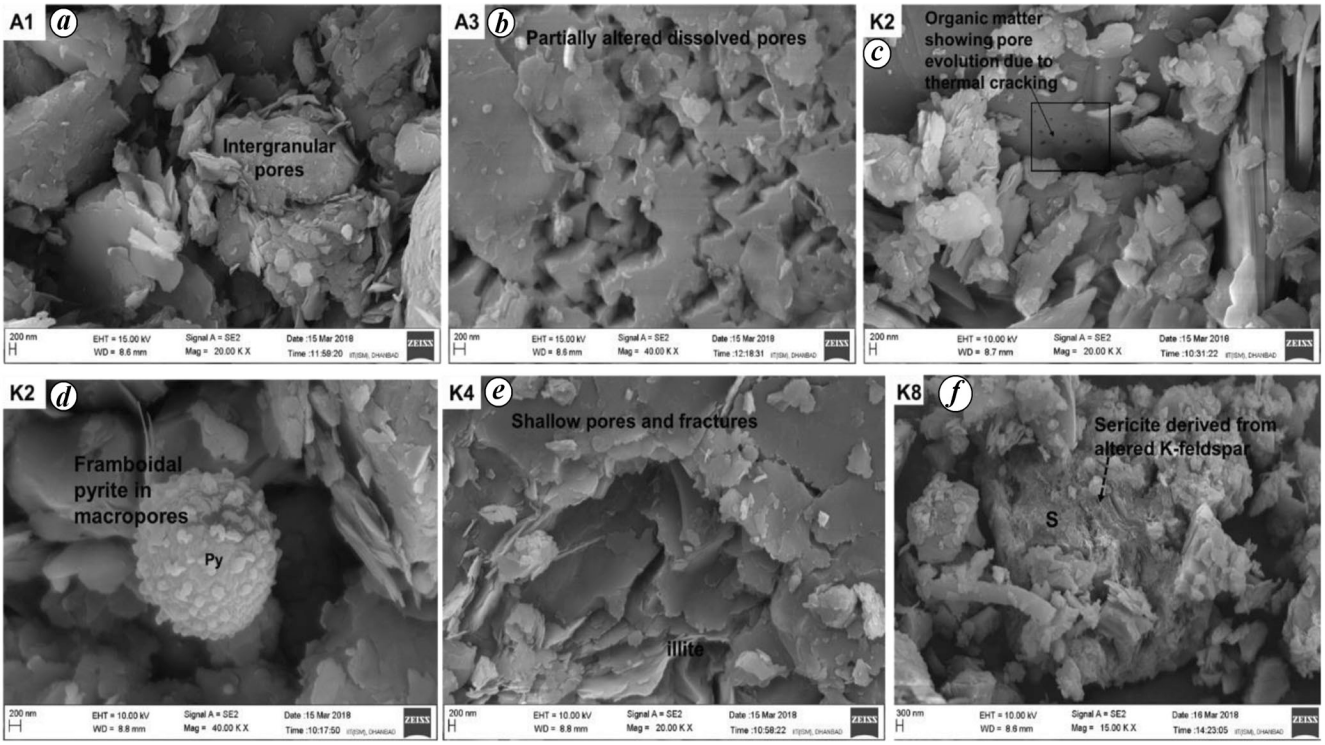


**Figure 5.** FE-SEM photomicrographs from Mizoram showing mainly (***a***) intergranular pores, (***b***) partially altered dissolved pores, (***c***) organic matter showing pore evolution due to thermal cracking, (***d***) framboidal pyrite (Py) in macropores, (***e***) illite in shallow pores and fractures and (***f***) sericite (S) features derived from altered orthoclase feldspar.

**Table 2.** Mineral abundance determined by X-ray diffraction in the samples of Upper Assam

| | | Mineralogical composition relative percentage (%) | | | | | | Clay minerals (%) | | |
|---|---|---|---|---|---|---|---|---|---|---|
| Sample | Depth (m) | Quartz | Albite | Orthoclase | Carbonate | Muscovite | Heavy minerals | Illite | Chlorite | Kaolinite |
| Well B1 | | | | | | | | | | |
| W1 | 4068.1–4068.2 | 46.0 | 13.0 | 14.3 | – | – | 3.9 | 18.4 | 2.1 | 2.2 |
| W2 | 4060.4–4060.5 | 55.7 | 14.7 | 6.20 | – | 4.9 | 8.0 | 6.6 | – | 3.9 |
| W3 | 4059.8–4059.9 | 35.9 | 13.9 | 11.4 | – | 10.6 | 9.1 | – | – | 19.1 |
| W4 | 4061.4–4061.5 | 41.5 | 11.4 | 3.5 | 4.9 | 3.4 | 7.9 | 4.2 | – | 23.2 |
| W5 | 4064.6–4064.7 | 29.9 | 23.4 | – | – | 7.2 | 7.0 | – | 19.0 | 13.6 |
| Well M5 | | | | | | | | | | |
| W6 | 2681.8–2682.0 | 49.5 | 20.1 | – | 5.2 | 6.8 | 2.8 | 2.4 | – | 13.3 |
| W7 | 2689.7–2689.8 | 42.7 | 5.8 | 14.7 | – | 14 | 2.1 | 13.3 | – | 5.5 |
| W8 | 2686.3–2686.4 | 46.3 | 13.7 | – | – | 14.5 | 6.3 | – | – | 19.2 |
| W9 | 2686.8–2686.9 | 50.2 | 20.7 | – | 8.7 | 9.0 | 2.3 | 3.7 | – | 5.3 |
| W10 | 2683.7–2683.8 | 31.8 | 26.4 | 14.8 | 7.6 | 5.8 | 2.4 | 17.9 | – | 9.0 |

The pore orientation, centroid of pores, pore structure, pore deepness and pore throat were stimulated to model the 3D pore network (Figure 7 *e*). The 3D visuals indicate the diversified pore distribution on a microscale considering pore depth and pore diameter. W2 and W6 show the directional pore network of fissile structure. A2 possesses a limited pore network, while K4 shows a shallow pore network connected to cracks/fractures. The pore network model indicates complex connectivity due to pore size and irregular heights attributed to the organic and inorganic heterogenic materials.

The virtual rock porosity was calculated using the extracted pore area from FE-SEM images. The porosity can be calculated by quantifying the dark and light pixels of these images using area proportion as follows[19]

$$\text{Porosity from image} \cong \frac{\text{Area occupied by pores}}{\text{Total area of the image}}.$$

Figure 8 shows the outcome of this 2D porosity from the FE-SEM images. The porosity varied from 8% to 19% in

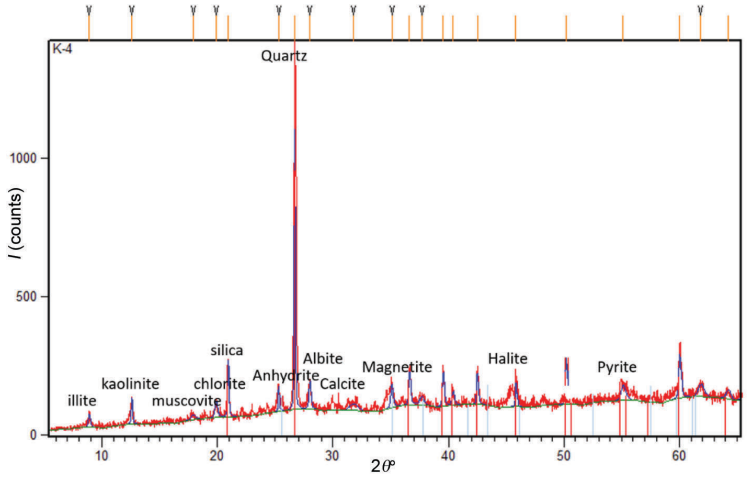


**Figure 6.** Typical example of interpreted X-ray diffractograms of sample K4 illustrating mineral composition.

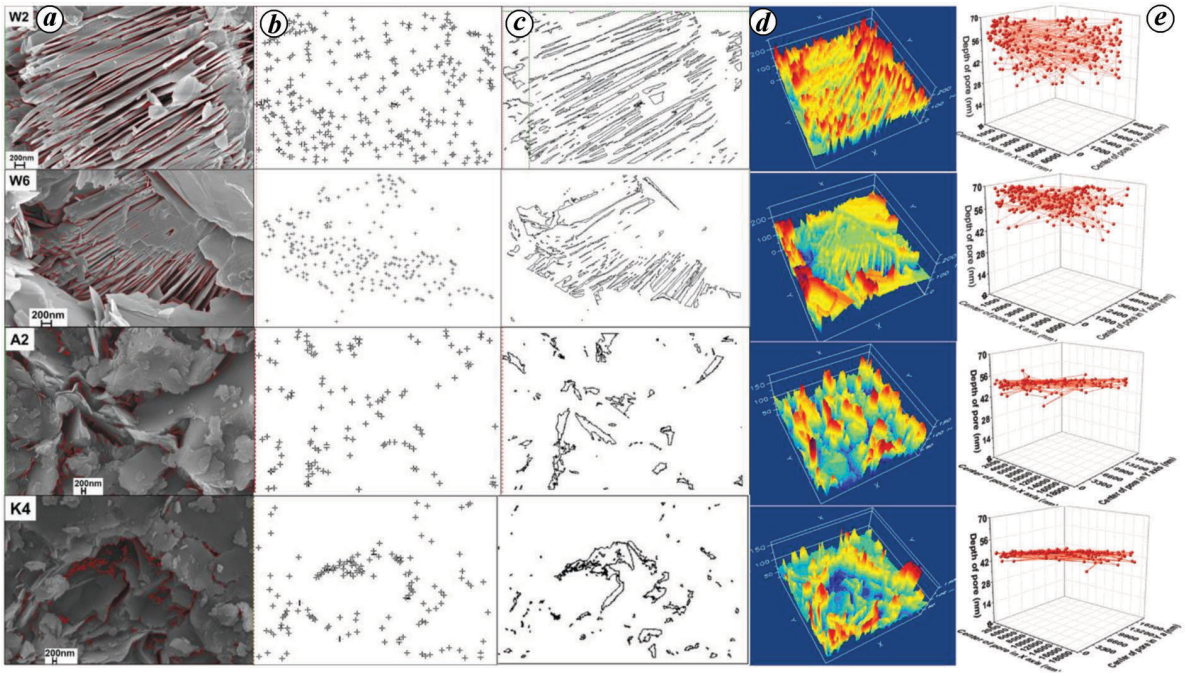


**Figure 7.** (***a***) FE-SEM photomicrograph with marked pores, (***b***) centroid of the pores and (***c***) pore structure and orientation, (***d***) 3D visualization for pore connectivity (from red to blue, the colour scale gradually shows increasing depth of pore), and (***e***) pore network of samples from Upper Assam (W2, W6) and Mizoram (A2, K4).

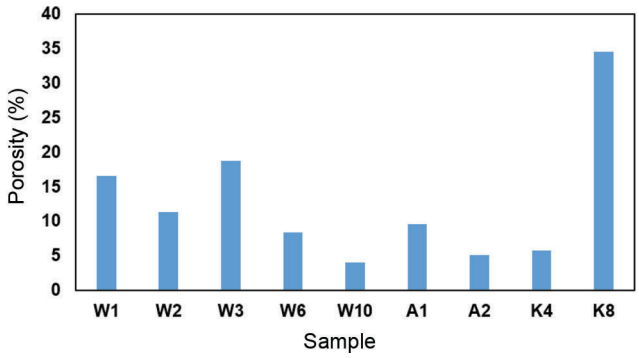


**Figure 8.** Porosity obtained from FE-SEM image digitization.

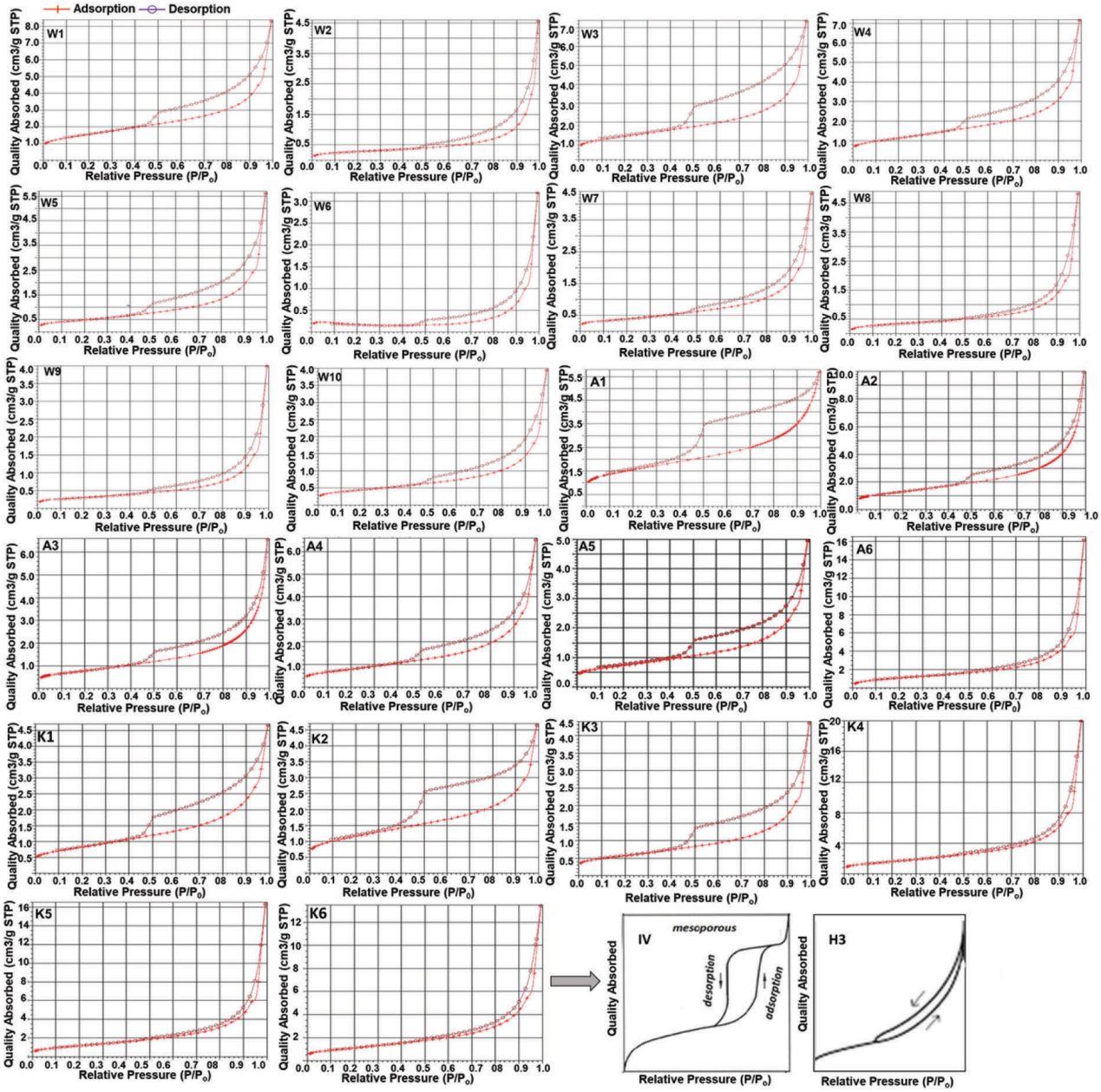


**Figure 9.** Nitrogen isotherms hysteresis loop for the samples from Upper Assam and Mizoram, which resembles type IV isotherms with H3 hysterosis loop.

the two wells of Upper Assam and from 9% to 35% in the two wells of Mizoram.

### *Pore size distribution from low-pressure $N_2$ adsorption analysis*

Pore size distribution (PSD) is the distribution of pore volume with respect to pore size. Gas adsorption provides a quantitative method to determine pore type, pore size, pore volume and PSD from a specific surface area, which helps in the reservoir quality estimation. The shape of the isotherm and its hysteresis pattern are related to the underlying adsorption mechanism, i.e. the interactions of solid and gas, and provide useful information about the type of pore structure present in the adsorbent[20]. The adsorption isotherms are classified into six types: I to VI (ref. 1). Type-IV isotherms are associated with dominantly meso- to macroporous materials. Type-IV isotherms are associated with the hysteresis loop, categorized into four hysteresis patterns (types H1 to H4) by IUPAC[1]. Each of these hysteresis patterns is characteristic of different shapes of the mesopore. Figure 9 shows the type-IV isotherm associated with hysteresis pattern H3 for the studied samples. The micropores are filled at low relative pressures, whereas

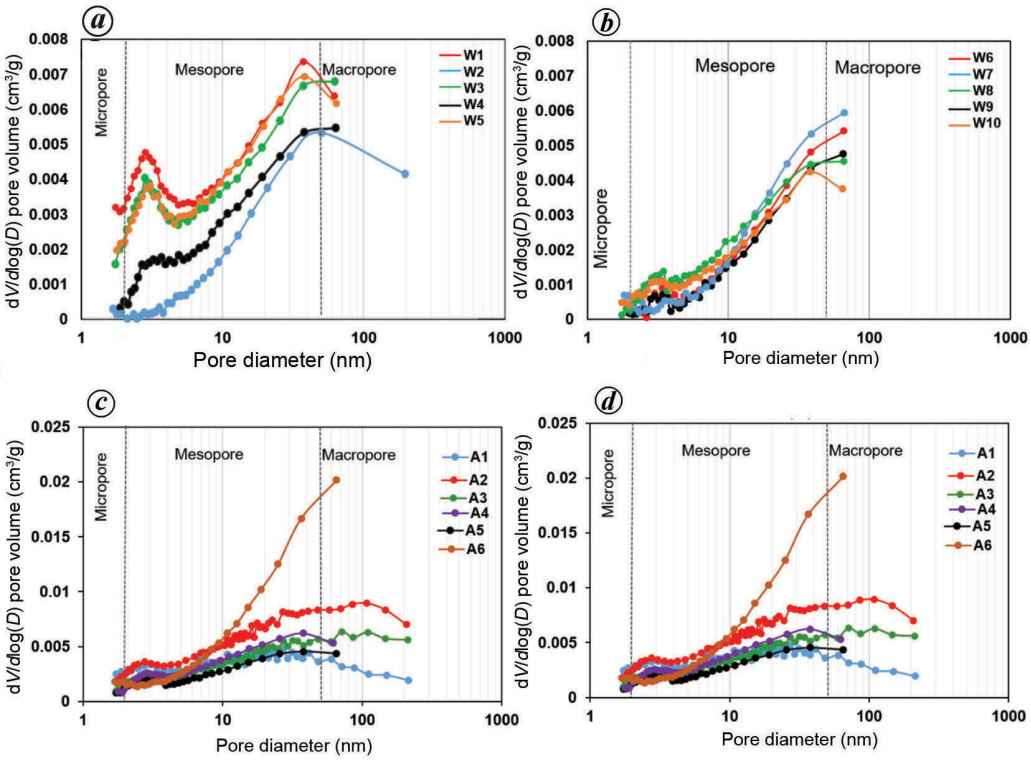


**Figure 10.** Pore size distribution (PSD) of micropores, mesopores and part of macropores obtained from gas adsorption analysis using incremental pore volume for the wells (***a***) B1 and (***b***) M5 in Upper Assam and wells (***c***) A and (***d***) K in Mizoram. Nitrogen PSD spectra are colour-coded separately for each sample of specific depth.

**Table 3.** Results of nitrogen adsorption measurement in Upper Assam and Mizoram

| Sample | Depth (m) | Brunauer–Emmet–Teller surface area ($m^2/g$) | Barrett, Joyner and Halenda (BJH) cumulative adsorption pore volume ($cm^3/100g$) | BJH adsorption average pore width (nm) |
|---|---|---|---|---|
| Well B1 | | | | |
| W1 | 4068.1–4068.2 | 5.4551 | 1.270484 | 11.318 |
| W2 | 4060.4–4060.5 | 1.0050 | 0.875125 | 30.421 |
| W3 | 4059.8–4059.9 | 4.0290 | 1.080608 | 12.435 |
| W4 | 4061.4–4061.5 | 1.7677 | 0.913176 | 18.300 |
| W5 | 4064.6–4064.7 | 4.3680 | 0.871697 | 12.058 |
| Well M5 | | | | |
| W6 | 2681.8–2682.0 | 1.3671 | 1.782376 | 35.054 |
| W7 | 2689.7–2689.8 | 1.2742 | 1.006066 | 23.795 |
| W8 | 2686.3–2686.4 | 1.4434 | 0.776452 | 17.774 |
| W9 | 2686.8–2686.9 | 1.0731 | 0.794919 | 24.700 |
| W10 | 2683.7–2683.8 | 1.6017 | 0.625512 | 17.231 |
| Well A | | | | |
| A1 | 1340–1344 | 5.4659 | 0.613489 | 9.410 |
| A2 | 1405–1406 | 4.6814 | 1.212297 | 14.657 |
| A3 | 1745–1750 | 2.8025 | 0.804312 | 15.552 |
| A4 | 2102–2104 | 2.8510 | 0.617725 | 13.222 |
| A5 | 3586–3588 | 2.5858 | 0.840316 | 14.258 |
| A6 | 3160–3162 | 4.0625 | 2.100319 | 23.422 |
| Well K | | | | |
| K1 | 545–550 | 2.9123 | 0.577990 | 11.071 |
| K2 | 730–735 | 4.0151 | 0.543329 | 9.224 |
| K3 | 1100–1102 | 2.0145 | 0.545477 | 14.763 |
| K4 | 1260–1262 | 7.4043 | 3.234985 | 19.568 |
| K5 | 1460–1462 | 4.3959 | 2.093641 | 21.179 |
| K6 | 2108–2110 | 4.1328 | 1.725544 | 18.614 |

the adsorption isotherm increases rapidly near $P/P_0 = 1$ due to the presence of macropores in the samples. The size and shape of the hysteresis loop can be used to obtain details about the pore types encountered by $N_2$ during a sorption experiment. Pore networks with narrow pore openings are represented by a broader plateau region of the hysteresis loop at higher $P/P_0$. Slit-shaped pores are characterized by a narrow hysteresis loop. The loops shown in Figure 9 are associated with slit shape and cylindrical open pores[21]. PSD of micropores, mesopores and part of macropores obtained from the gas adsorption analysis using incremental pore volume is displayed in Figure 10 for samples of wells B1, M5, A and K. B1 shows high amplitudes near small microscope (<10 nm), large mesospore and macropore range (≥50 nm). However, M5 shows a slight increase in amplitude near 2–3 nm and follows the same pattern for all the five samples. Table 3 summarizes the collected results from low-pressure $N_2$ adsorption measurements, including BET surface area, total cumulative pore volume and calculated average pore width. The adsorption results indicate an inverse relationship between surface area and pore size. Thus, small pore sizes, i.e. high surface area, may correspond to high irreducible water saturation. Considering the importance of surface area, the flow mechanism supported by mesopores is important for reservoir characterization.

## Conclusion

Pore structure plays a crucial role in controlling the physical properties of rocks and stored fluids. Pore-scale study will aid in future exploration and production strategies in unexploited tight sands and mature oil fields of the Assam–Arakan Basin. The pore-scale evaluation of reservoir rocks of the Barail Arenaceous Formation of the Oligocene and the Bhuban Formation of the Early Miocene is discussed in this study, considering the mineralogical composition, pore structure and pore distribution. The following observations are drawn from the study:

(a) Petrographic study helps in understanding the mineral composition of rocks, cementation and environment of deposition by observing the sorting pattern. Most of the samples are medium to fine-grained and poorly sorted. The shape, size and sorting of grains from petrographic study directly impact the porosity and permeability of a reservoir. These properties are dependent on the connectivity and structure of the pore spaces.

(b) Quartz, feldspar, muscovite, pyrite, clay minerals, mainly kaolinite and illite, are identified from petrography, FE-SEM and XRD analyses. The presence of intergranular pores indicates that the samples have excellent porosity and interconnected pores, which may support the flow mechanism. However, the partially filled macropores with books of kaolinite sometimes reduce permeability in porous media.

(c) In order to visualize pore connectivity, which contributes to fluid flow, the 3D pore network model was simulated. It illustrates the pore surface morphology with the spatial distribution of pores. The micro-, meso- and macropores were well connected with moderate to excellent pore network, which may be helpful for flow mechanism.

(d) PSD from $N_2$ adsorption analysis revealed that the study area is dominated by mesopores and macropores. The shape of the adsorption–desorption isotherm curves indicates type-IV with H3 hysteresis loop, which is associated with plate-like particles, e.g. some clays.


1. Sing, K. S. W., Everett, D. H., Haul, R. A. W., Moscou, L., Pierotti, R. A., Rouquerol, J. and Siemieniewska, T., Reporting physisorption data for gas/solid systems with special reference to the determination of surface area and porosity. *Pure Appl. Chem*., 1985, **57**, 603–619.
2. Kuila, U. and Prasad, M., Specific surface area and pore-size distribution in clays and shales. *Geophys. Prospect.,* 2013, **61**, 341–362.
3. Wandrey, C. J., Sylhet–Kopili/Barail–Tipam composite total petroleum system, Assam Geologic Province, India. *US Geol. Surv. Bull.*, 2004, **2208-D**, 1–19.
4. Alam, J., Chatterjee, R. and Dasgupta, S., Estimation of pore pressure, tectonic strain and stress magnitudes in the Upper Assam basin: a tectonically active part of India. *Geophys. J. Int.*, 2019, **216**, 659–675.
5. Gogoi, T. and Chatterjee, R., Estimation of petrophysical parameters using seismic inversion and neural network modeling in Upper Assam basin, India. *Geosci. Front.*, 2019, **10**(3), 1113–1124; https://doi.org/10.1016/j.gsf.2018.07.002.
6. Murty, K. N., Geology and hydrocarbon prospects of Assam Shelf – recent advances and present status. *Petrol. Asia J.*, 1983, **6**(4), 1–14.
7. Lokho, K. and Singh, B. P., Ichnofossils from the Miocene Middle Bhuban Formation, Mizoram, Northeast India and their paleoenvironmental significance. *Acta Geol. Sin.*, 2013, **87**(4), 801–812.
8. Nandy, D. R., Dasgupta, S., Sarkar, K. and Ganguly, A., Tectonic evolution of Tripura–Mizoram Fold Belt, Surma Basin, northeast India. *J. Geol. Min. Metall. Soc. India*, 1983, **55**(4), 186–194.
9. Gogoi, T. and Chatterjee, R., Multimineral modeling and estimation of brittleness index of shaly sandstone in Upper Assam and Mizoram areas, India. *SPE Reserv. Eval. Eng*., 2020, **23**(2), 708–721; https://doi.org/10.2118/200498-PA.
10. Welton, J. E., *SEM petrology Atlas*, American Association of Petroleum Geologists, Oklahoma, USA, 2003, p. 247.
11. Mendhe, V. A. *et al.*, Geochemical and petrophysical characteristics of Permian shale gas reservoirs of Raniganj Basin, West Bengal, India. *Int. J. Coal Geol.*, 2018, **188**, 1–24.
12. Brunauer, S., Emmett, P. H. and Teller, E., Adsorption of gases in multimolecular layers. *J. Am. Chem. Soc.*, 1938, **60**(2), 309–319.
13. Nelson, P. H., Pore-throat sizes in sandstones, tight sandstones, and shales. *AAPG Bull.*, 2009, **93**, 329–340.
14. Barett, E. P., Joyner, L. G. and Halenda, P. P., The determination of pore volume and area distributions in porous substances, I. Computations from nitrogen isotherms. *J. Am. Chem. Soc.*, 1951, **73**(1), 373–380.
15. Wu, K., Ma, Q. F. and Feng, Q. I., Middle Permian pore characteristics and shale gas exploration significance from the Gu-feng formation in Jianshi, Western Hubei. *Earth Sci. J. China Univ. Geosci*., 2012, **37**, 175–183.
16. Tavanaei, A. and Salehi, S., Pore, throat, and grain detection for rock SEM images using digital watershed image segmentation algorithm. *J. Porous Media*, 2015, **18**, 507–518.
17. Fatt, I. *et al.*, The network model of porous media. *Petrol. Trans. AIME*, 1956, **207**, 160–181.

18. Mendhe, V. A., Mishra, S., Kamble, A. D., Bannerjee, M., Mukherjee, S., Kumar, V. and Sinha, A., Shale gas and emerging energy resource: prospects in India. *Indian Min. Eng. J*., 2015, **54**(6), 21–31.
19. Sarkar, P., Kumara, A., Singh, K. H., Ghosh, R. and Singh, T. N., Pore system, microstructure and porosity characterization of Gondwana shale of Eastern India using laboratory experiment and watershed image segmentation algorithm. *Mar. Pet. Geol.*, 2018, **94**, 246–260.
20. Anovitz, L. M. and Cole, D. R., Characterization and analysis of porosity and pore structures. *Rev. Mineral. Geochem.*, 2015, **80**, 61–164; http://dx.doi.org/10.2138/rmg.2015.80.04.
21. Brunauer, S., Deming, L. S., Deming, W. S. and Teller, E., On a theory of the Van der Waals adsorption of gases. *J. Am. Chem. Soc*., 1940, **62**, 1723–1732.

ACKNOWLEDGEMENTS. We thank Oil India Limited, Duliajan, for providing the necessary data to carry out this work; CSIR-Central Institute of Mining and Fuel Research, Dhanbad, for providing the access to the image processing software; the Department of Applied Geology, Indian Institute of Technology (Indian School of Mines) (IIT(ISM)), Dhanbad for providing the necessary facilities for the petrographic study and Central Research Facility (CRF), IIT(ISM) Dhanbad, CRF, IIT Kharagpur and Indian Association for the Cultivation of Science, Jadavpur for carrying out various laboratory analyses. We also thank Ministry of Earth Sciences, Government of India for funds (MoES/P.O.(Seismo)/1(273)/2015).

Received 10 January 2022; revised accepted 2 May 2022

doi: 10.18520/cs/v123/i2/202-213